Nuclear dynamics at the balance energy of mass asymmetric colliding nuclei.

Supriya Goyal

House No. 86, Phase-III, Urban Estate, Dugri Road, Ludhiana, Punjab - 141 013, India.

Abstract

Using the quantum molecular dynamics model, we study the nuclear dynamics at the balance energy of mass asymmetric colliding nuclei by keeping the total mass of the system fixed as 40, 80, 160, and 240. The calculations are performed by varying the mass asymmetry ($\eta = \frac{A_T - A_P}{A_T + A_P}$; where A_T and A_P are the masses of the target and projectile, respectively) of the reaction from 0.1 to 0.7. In particular, we study the various quantities like average and maximum density, collision rate, participant-spectator matter, anisotropic ratio, relative momentum as well as their mass asymmetry and mass dependence. We find sizeable effects of mass asymmetry on these quantities. Our results indicate that the mass dependence of various quantities increases slightly with increase in η.

Keywords: heavy-ion collisions, quantum molecular dynamics (QMD) model, balance energy, mass asymmetric reactions, nuclear dynamics

1. Introduction

It is now well established that collective transverse flow of the nucleons is a signature of the interaction and can provide information about the equation of state (EoS) as well as nucleon-nucleon (nn) cross-section of the nuclear matter. Extensive studies have been done over the past three decades on the sensitivity of collective transverse flow towards the nuclear EoS, nn cross-section as well as entrance channel parameters such as incident energy of projectile, size of the system ($A_{TOT} = A_T + A_P$) and colliding geometry (i.e.

Email address: supriyagoyal.pu@gmail.com,ashuphysics@gmail.com (Supriya Goyal)

Preprint submitted to Physics Letters B *June 21, 2011*

impact parameter) [1, 2, 3, 4, 5, 6]. The disappearance of flow is predicted to appear at some incident energy, which is termed as Balance Energy (E_{bal}) [7]. This balance energy has been subjected to extensive theoretical and experimental calculations to known its accurate value as well as its mass and impact parameter dependence [8, 9, 10, 11, 12].

Recently, the sensitivity of collective transverse flow and E_{bal} towards the mass asymmetry of the reaction has been carried out at different colliding geometries by keeping the total mass of the system fixed [11, 12]. It has been found that almost independent of total system mass as well as colliding geometry, mass asymmetry has a uniform effect on the collective transverse flow and its disappearance [11]. This study was motivated from the recent observations by FOPI collaboration on the mass asymmetric reactions of ^{40}Ca+^{197}Au and ^{197}Au+^{40}Ca [13]. They observe that flow in asymmetric reactions is a key observable for investigating the reaction dynamics. The difference between the reaction dynamics for symmetric and asymmetric reactions is attributed to the different role played by excitation energy in these reactions. In symmetric reactions most of the excitation energy is deposited in the form of compressional energy, whereas an asymmetric reaction deposit it in the form of thermal energy [14]. Therefore, in the present paper this study is further extended for the central collisions to see the effect of mass asymmetry of the reaction on the nuclear dynamics at the balance energy. Similar work has been carried out by Sood and Puri [15] for the nearly symmetric and symmetric reactions at the balance energy. But the role of mass asymmetry on the participant-spectator matter, average and maximum density, net collisions, anisotropic ratio, relative momentum as well as on the mass dependence of these quantities is not taken care of. This has been taken care in the present study. The study is made within the framework of Quantum Molecular Dynamics (QMD) model [9, 11, 12, 14, 15, 16, 17, 18], which is explained in section 2. Results and discussion are explained in section 3 and finally we summarizes the results in section 4.

2. The quantum molecular dynamics model

The quantum molecular dynamics model [9, 11, 12, 14, 15, 16, 17, 18] simulates the reaction on an event by event basis. Here each nucleon i is represented by a Gaussian wave packet with a width of $\sqrt{L}$ centered around the mean position $\vec{r}_i$(t) and mean momentum $\vec{p}_i$(t). Here each nucleon is represented by a coherent state of the form:

$$\phi_i(\vec{r}, \vec{p}, t) = \frac{1}{(2\pi L)^{3/4}} e^{\left[-\{\vec{r}-\vec{r}_i(t)\}^2/4L\right]} e^{[i\vec{p}_i(t)\cdot\vec{r}/\hbar]}. \quad (1)$$

The Wigner distribution of a system with $A_T + A_P$ nucleons is given by

$$f(\vec{r}, \vec{p}, t) = \sum_{i=1}^{A_T+A_P} \frac{1}{(\pi\hbar)^3} e^{\left[-\{\vec{r}-\vec{r}_i(t)\}^2/2L\right]} e^{\left[-\{\vec{p}-\vec{p}_i(t)\}^2 2L/\hbar^2\right]'}, \quad (2)$$

with L = 1.08 fm^2.

The center of each Gaussian (in the coordinate and momentum space) is chosen by the Monte Carlo procedure. The momentum of nucleons (in each nucleus) is chosen between zero and local Fermi momentum [= $\sqrt{2m_i V_i(\vec{r})}$; $V_i(\vec{r})$ is the potential energy of nucleon i]. Naturally, one has to take care that the nuclei, thus generated, have right binding energy and proper root mean square radii.

The centroid of each wave packet is propagated using the classical equations of motion:

$$\frac{d\vec{r}_i}{dt} = \frac{dH}{d\vec{p}_i}, \quad (3)$$

$$\frac{d\vec{p}_i}{dt} = -\frac{dH}{d\vec{r}_i}, \quad (4)$$

where the Hamiltonian is given by

$$H = \sum_i \frac{\vec{p}_i^2}{2m_i} + V^{tot}. \quad (5)$$

Our total interaction potential V^{tot} reads as

$$V^{tot} = V^{Loc} + V^{Yuk} + V^{Coul} + V^{MDI}, \quad (6)$$

with

$$V^{Loc} = t_1\delta(\vec{r}_i - \vec{r}_j) + t_2\delta(\vec{r}_i - \vec{r}_j)\delta(\vec{r}_i - \vec{r}_k), \quad (7)$$

$$V^{Yuk} = t_3 e^{-|\vec{r}_i-\vec{r}_j|/m} / \left(|\vec{r}_i - \vec{r}_j|/m\right), \quad (8)$$

with m = 1.5 fm and t_3 = -6.66 MeV.

The static (local) Skyrme interaction [19] can further be parametrized as:

$$U^{Loc} = \alpha \left(\frac{\rho}{\rho_o}\right) + \beta \left(\frac{\rho}{\rho_o}\right)^{\gamma}. \tag{9}$$

Here α, β and γ are the parameters that define equation of state. The momentum dependent interaction is obtained by parameterizing the momentum dependence of the real part of the optical potential. The final form of the potential reads as

$$U^{MDI} \approx t_4 ln^2[t_5(\vec{p}_i - \vec{p}_j)^2 + 1]\delta(\vec{r}_i - \vec{r}_j). \tag{10}$$

Here t_4 = 1.57 MeV and t_5 = 5 $\times 10^{-4} MeV^{-2}$. A parameterized form of the local plus momentum dependent interaction (MDI) potential (at zero temperature) is given by

$$U = \alpha \left(\frac{\rho}{\rho_0}\right) + \beta \left(\frac{\rho}{\rho_0}\right) + \delta ln^2[\epsilon(\rho/\rho_0)^{2/3} + 1]\rho/\rho_0. \tag{11}$$

The parameters α, β, and γ in above Eq. (11) must be readjusted in the presence of momentum dependent interactions so as to reproduce the ground state properties of the nuclear matter. The set of parameters corresponding to different equations of state can be found in Ref. [17].

3. Results and discussion

For the present analysis, we simulated the reactions of ${}^{17}_{8}O +^{23}_{11} Na$ ($\eta = 0.1$), ${}^{14}_{7}N +^{26}_{12} Mg$ ($\eta = 0.3$), ${}^{10}_{5}B +^{30}_{14} Si$ ($\eta = 0.5$), and ${}^{6}_{3}Li +^{34}_{16} S$ ($\eta = 0.7$) for $A_{TOT} = 40$, ${}^{36}_{18}Ar +^{44}_{20} Ca$ ($\eta = 0.1$), ${}^{28}_{14}Si +^{52}_{24} Cr$ ($\eta = 0.3$), ${}^{20}_{10}Ne +^{60}_{28} Ni$ ($\eta = 0.5$), and ${}^{10}_{5}B +^{70}_{32} Ge$ ($\eta = 0.7$) for $A_{TOT} = 80$, ${}^{70}_{32}Ge +^{90}_{40} Zr$ ($\eta = 0.1$), ${}^{54}_{26}Fe +^{106}_{48} Cd$ ($\eta = 0.3$), ${}^{40}_{20}Ca +^{120}_{52} Te$ ($\eta = 0.5$), and ${}^{24}_{12}Mg +^{136}_{58} Ce$ ($\eta = 0.7$) for $A_{TOT} = 160$, and ${}^{108}_{48}Cd +^{132}_{56} Ba$ ($\eta = 0.1$), ${}^{84}_{38}Sr +^{156}_{66} Dy$ ($\eta = 0.3$), ${}^{60}_{28}Ni +^{180}_{74} W$ ($\eta = 0.5$), and ${}^{36}_{18}Ar +^{204}_{82} Pb$ ($\eta = 0.7$) for $A_{TOT} = 240$, at their corresponding theoretical balance energies (taken from Ref. [11]). The balance energies at which these reactions are simulated were calculated using a momentum dependent soft equation of state with standard energy dependent cugnon cross-section and reduced impact parameter ($\hat{b} = \frac{b}{b_{max}}$; where $b_{max} = R_1 + R_2$; R_i is the radius of projectile or target) of 0.25. The reactions are followed uniformly up to 500 fm/c.

In Fig. 1, we display the $\langle\rho^{avg}\rangle/\rho_0$ (left column) and $\langle\rho^{max}\rangle/\rho_0$ (right column) as a function of the reaction time. The average $\langle\rho^{avg}\rangle$ and maximal $\langle\rho^{max}\rangle$ values of the density are calculated within a sphere of radius 2 fm around the center-of-mass. The density is then computed at each time step during the reaction using equation:

$$\rho(\vec{r},t) = \sum_{i=1}^{A_T+A_P} \frac{1}{(2\pi L)^{3/2}} e^{(-(\vec{r}-\vec{r}_i(t))^2/2L)}. \tag{12}$$

The results are displayed by varying η from 0.1 to 0.7 for different mass ranges i.e A_{TOT} = 40, 80, 160, and 240. It is clear from the figure that the maximal ρ^{avg} decreases with increase in η. A similar trend can be seen for the evolution of ρ^{max} at all mass ranges. This is due to the decrease in the interaction region with increase in mass asymmetry of the reaction. Further, one should note that for nearly symmetric reactions with $\eta = 0.1$, the maximal and average densities are comparable for the heavy systems, indicating the wide and uniform formation of dense matter in the central region of 2 fm radius. This is similar to as predicted in Ref. [15]. However, a nonhomogeneous nature of the dense matter is seen for lighter systems at all asymmetries. For each mass range, as η increases and for each η, as A_{TOT} decreases, the incident energy increases. Therefore, for each A_{TOT}, the reactions with larger asymmetries and for each η, the systems with smaller A_{TOT}, finishes much earlier. Similarly, the peak values of the densities are also delayed for reactions of heavy colliding nuclei and smaller asymmetries. Also, one should note that the time of saturation increases with increase in η.

Similar to Fig. 1, we display the net collision rate as a function of the reaction time in Fig. 2. It is directly connected with the density. Due to the decrease in interaction volume with increase in mass asymmetry of colliding nuclei, the net collision rate decreases with increase in η and the interactions among nucleons also ceases earlier. This is observed for all system mass ranges. As expected, with increase in system mass, opposite trend is observed for each η. This behavior is also evident from the density profile (see Fig. 1).

It is well known that balance energy represents a counterbalancing between the attractive and repulsive forces, therefore, this fact should also be reflected in quantities like spectator and participant matter. In Fig. 3, we display the normalized spectator (upper panel) and participant (lower panel) matter as a function of reaction time. The results are displayed for different asymmetries by keeping the total mass of the system fixed as $A_{TOT} = 80$ and 240. All nucleons having experienced at least one collision are termed as participant and the remaining matter is termed as spectator matter. One can also define spectator and participant matter in terms of rapidity distribution, however, the results are similar for both definitions, as shown in Ref. [15]. From the figure, one clearly see that at the start of the reaction, all nucleons constitute spectator matter, therefore, no participant matter exists at initial time (i.e. t = 0 fm/c). Due to decrease in the number of nn collisions with increase in η, the spectator(participant) matter increases(decreases) with increase in η. Similar behavior is seen for different system masses.

In Fig. 4, we display the time evolution of relative momentum $< K_R >$ (left column) and anisotropy ratio $< R_a >$ (right panel) for different η and A_{TOT}. The relative momentum is the indicator of local equilibrium while anisotropy ratio is the indicator of the global equilibrium reached in the heavy-ion reactions. The details of these quantities can be found in Ref. [18]. From figure, we see that relative momentum decreases as the reaction proceeds, while $< R_a >$ ratio increases and saturates after the high dense phase is over. Due to increase in incident energy with η, thermalization is little bit better achieved for larger η. Similar behavior is observed for each fixed system mass. However for each η, due to high density obtained in heavier systems, the thermalization is better achieved compared to lighter colliding nuclei.

In Fig. 5, we display the mass asymmetry dependence of the maximal value of the average and maximum density as well as the final stage value of (allowed) nn collisions and spectator/participant matter. The results are displayed for different mass ranges. Lines are the linear fits ($\propto m\eta$). We find that the maximal values of the average and maximum density decreases with increase in η for each fixed system mass and the η dependence decreases with increase in system mass. An opposite trend is observed for nn collisions. The nn collisions also decreases with increase in η, but due to larger interaction volume in heavier systems, heavier colliding nuclei show large η dependence. Obviously, the spectator matter and the participant matter will behave oppositely. For each system mass, the spectator(participant) matter increases(decreases) with increase in η and similar to density, the η dependence decreases with increase in total mass of the system. From this figure, it is clear that mass asymmetry of the reaction has a significant role on the nuclear dynamics of the reaction. Therefore, while studying various phenomenon in the intermediate energy heavy-ion collisions, one should take care of the mass asymmetry of the reaction.

In Fig. 6, we display the mass dependence of the maximal value of the average and maximum density as well as the final stage value of (allowed) nn collisions and spectator/participant matter. For the nearly symmetric reaction having $\eta = 0.1$, the dependence is similar to that shown in Ref. . All the quantities follow a power law behavior $\propto A_{TOT}^{\tau}$. The values of power factor τ are displayed in the figure. A slight decrease in the average density with increasing size of the system is observed for nearly symmetric reaction with $\eta = 0.1$, whereas a opposite trend is seen for η = 0.3-0.7. Similarly, a decrease in the maximum density with increasing size of the system is observed for reactions with η = 0.1-0.5, while a opposite trend is seen for $\eta = 0.7$. For nn collisions, one sees a linear enhancement with the system mass for each η. The spectator and participant matter is nearly independent of the mass of the system. As one look carefully, the mass dependence of various quantities shown in Fig. 6, increases slightly with increase in η.

4. Summary

We studied the nuclear dynamics (particularly, average and maximum density, collision rate, participant-spectator matter, anisotropic ratio, relative momentum as well as their mass asymmetry and mass dependence) at the balance energy of mass asymmetric reactions by keeping the total mass of the system fixed as 40, 80, 160, and 240 and varying the mass asymmetry of the reaction from 0.1 to 0.7. A sizeable effect of mass asymmetry on these quantities is observed. Our results clearly indicated that the mass dependence of various quantities increases slightly with increase in η.

5. Acknowledgement

Author is thankful to Dr. Rajeev K. Puri for interesting and constructive discussions. This work is supported by a research grant from the Council of Scientific and Industrial Research (CSIR), Govt. of India, vide grant no. 09/135(0563)/2009-EMR-1.

References

[1] W. Scheid, H. Müller, W. Greiner, Phys. Rev. Lett. 32 (1974) 741;
H. A. Gustafsson *et al.*, Phys. Rev. Lett. 52 (1984) 1590.

[2] C. A. Ogilvie *et al.*, Phys. Rev. C 40 (1989) 2592;
B. Blättel, V. Koch, A. Lang, K. Weber, W. Cassing, U. Mosel, Phys. Rev. C 43 (1991) 2728.

[3] A. Andronic *et al.*, Phys. Rev. C 67 (2003) 034907.

[4] J. Lukasik *et al.*, Phys. Lett. B 608 (2005) 223.

[5] Y. Zhang, Z. Li, Phys. Rev. C 74 (2006) 014602.

[6] B. Hong *et al.*, Phys. Rev. C 66 (2000) 034901;
J. Lukasik and W. Trautmann, Proc. International Nuclear Physics Conference (INPC2007), Vol. 2, p. 513.

[7] D. Krofcheck *et al.*, Phys. Rev. Lett. 63 (1989) 2028.

[8] D. J. Magestro *et al.*, Phys. Rev. C 61 (2000) 021602(R).

[9] S. Kumar, M. K. Sharma, R. K. Puri, K. P. Singh, I. M. Govil, Phys. Rev. C 58 (1998) 3494;
A. D. Sood, R. K. Puri, Phys. Lett. B 594 (2004) 260; Phys. Rev. C 69 (2004) 054612; Eur. Phys. J. A 30 (2006) 571; Phys. Rev. C 73 (2006) 067602; Phys. Rev. C 79 (2009) 064618;
R. Chugh, R. K. Puri, Phys. Rev. C 82 (2010) 014603.

[10] D. J. Magestro, W. Bauer, G. D. Westfall, Phys. Rev. C 62 (2000) 041603(R).

[11] S. Goyal, R. K. Puri, Nucl. Phys. A 853 (2011) 164.

[12] S. Goyal, Nucl. Phys. A 856 (2011) 154; Phys. Rev. C 83 (2011) 047604.

[13] O. Hartmann, Dissertation, TU Darmstadt (2003);
K. J. Eskola, Nucl. Phys. B 323 (1989) 37.

[14] J. Singh, Ph.D. Thesis, Panjab University, Chandigarh, India, (2001).

[15] A. D. Sood, R. K. Puri, Phys. Rev. C 70 (2004) 034611.

[16] S. W. Huang *et al.*, Phys. Lett. B 298 (1993) 41;
S. W. Huang *et al.*, Prog. Nucl. Part. Phys. 30 (1993) 105;
E. Lehmann *et al.*, Prog. Nucl. Part. Phys. 30 (1993) 219;

G. Batko *et al.*, J. Phys. G 20 (1994) 461;
E. Lehmann *et al.*, Phys. Rev. C 51 (1995) 2113;
C. Fucks, J. Phys. G 22 (1996) 131;
R. K. Puri *et al.*, Phys. Rev. C 54 (1996) 28;
C. Hartnack *et al.*, Eur. Phys. J. A 1 (1998) 151;
R. K. Puri *et al.*, Phys. Rev. C 57 (1998) 2744;
R. K. Puri *et al.*, J. Comp. Phys. 162 (2000) 245;
J. K. Dhawan *et al.*, Phys. Rev. C 75 (2007) 057601;
S. Kumar *et al.*, Phys. Rev. C 78 (2008) 064602;
Y. K. Vermani *et al.*, Eur. Phys. Lett. 85 (2009) 062001;
Y. K. Vermani *et al.*, J. Phys. G 36 (2009) 105103;
S. Kumar *et al.*, Phys. Rev. C 81 (2010) 014611;
S. Kumar *et al.*, Phys. Rev. C 81 (2010) 014601;
Y. K. Vermani *et al.*, J. Phys. G 37 (2010) 015105;
S. Gautam *et al.*, J. Phys. G 37 (2010) 085102;
S. Gautam *et al.*, Phys. Rev. C 83 (2011) 014603;
S. Gautam *et al.*, Phys. Rev. C 83 (2011) 034606;
W. Hauer *et al.*, Phys. Lett. B 697 (2011) 512;
S. Goyal, R. K. Puri, Phys. Rev. C 83 (2011) 047601.

[17] J. Aichelin, Phys. Rep. 202 (1991) 233.

[18] J. K. Dhawan, Ph.D. Thesis, Panjab University, Chandigarh, India, (2007).

[19] R. K. Puri *et al.*, Phys. Rev. C 43 (1991) 315;
R. K. Puri *et al.*, Phys. Rev. C 45 (1992) 1837;
R. K. Puri *et al.*, Eur. Phys. J. A 3 (1998) 277;
R. K. Puri *et al.*, Eur. Phys. J. A 8 (2000) 103;
R. K. Puri *et al.*, Eur. Phys. J. A 23 (2005) 429;
I. Dutt, R. K. Puri, Phys. Rev. C 81 (2010) 044615; Phys. Rev. C 81 (2010) 047601; Phys. Rev. C 81 (2010) 064609; Phys. Rev. C 81 (2010) 064608;
S. Kumar *et al.*, Chinese Phys. Lett. 27 (2010) 062504.

Figure Captions

FIG. 1. (Color Online) The time evolution of the average density $\langle \rho^{avg} \rangle / \rho_0$ (left column) and maximum density $\langle \rho^{max} \rangle / \rho_0$ (right column) reached in a central sphere of radius 2 fm for different system masses. The results for different asymmetries $\eta = 0.1$, 0.3, 0.5, and 0.7 are represented, respectively, by the solid, dashes, dotted and dashed-dotted lines.

FIG. 2. (Color Online) Same as Fig. 1, but the rate of allowed collisions versus reaction time.

FIG. 3. (Color Online) The time evolution of the normalized spectator matter (upper panel) and participant matter (lower panel). The results for total system mass $A_{TOT} = 80$ and 240 are displayed in left and right columns. Lines have the same meaning as in Fig. 1.

FIG. 4. (Color Online) Same as Fig. 1, but for the relative momentum $< K_R >$ (left column) and anisotropy ratio $< R_a >$ (right column).

FIG. 5. (Color Online) The maximal value of the average density $< \rho^{avg} >_{max}$ (left upper-panel), maximum density $< \rho^{max} >_{max}$ (right upper-panel), total number of the allowed collisions obtained at the final stage (left lower-panel), and final saturated spectator/participant matter (right lower-panel) as a function of mass asymmetry of the reaction. The results for different system masses $A_{TOT} = 40$, 80, 160, and 240 are represented, respectively, by the solid squares, circles, triangles and inverted triangles. Lines are the linear fits ($\propto m\eta$); m values without errors are displayed.

FIG. 6. (Color Online) Same as Fig. 5, but as a function of total mass of the system. The results for different asymmetries $\eta = 0.1$, 0.3, 0.5, and 0.7 are represented, respectively, by the open squares, circles, triangles and inverted triangles. The lines are power law ($\propto A_{TOT}^{\tau}$) fits to the calculated results. The values of the power factor τ are displayed in the figure for various quantities.

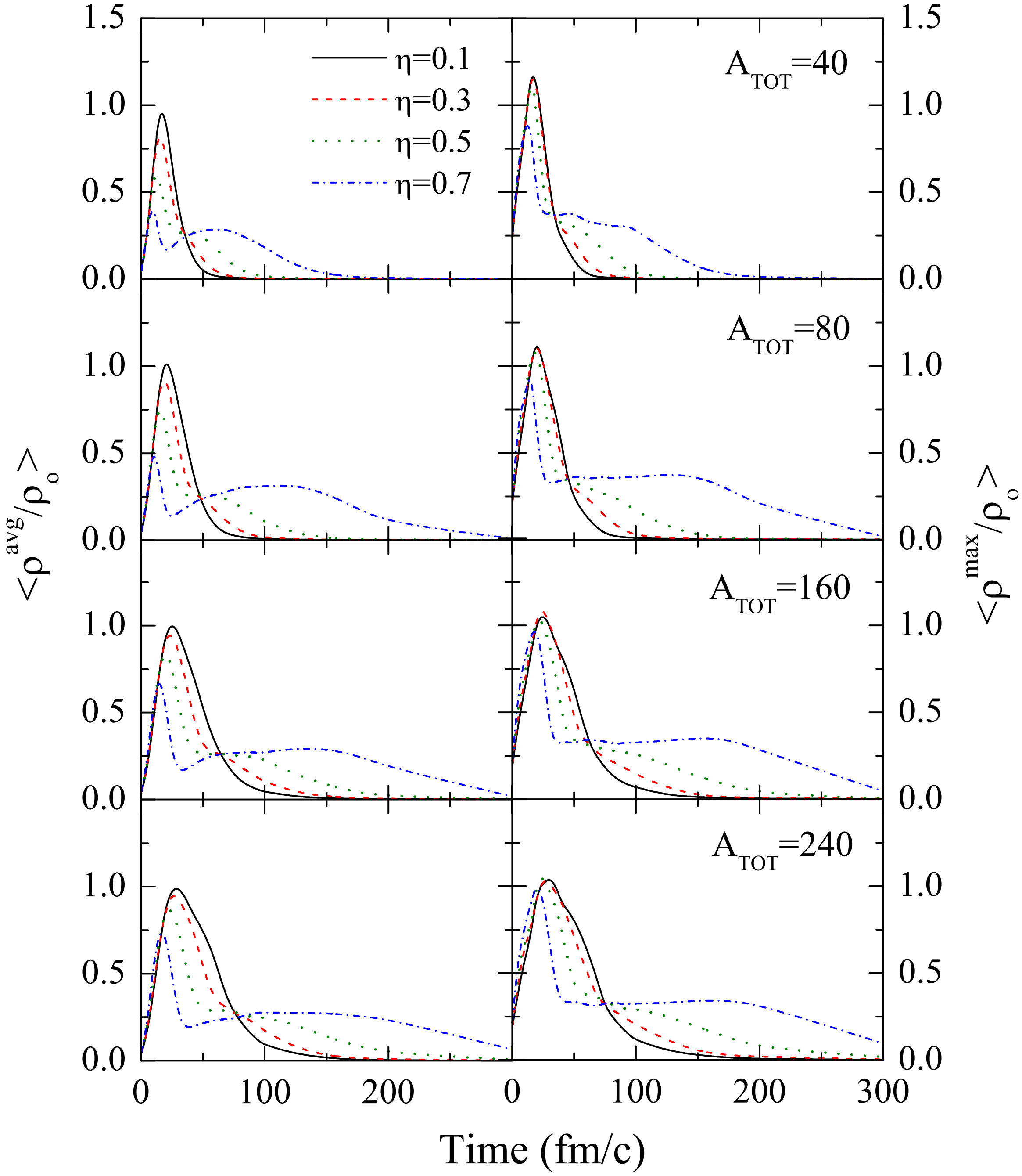

η=0.1
η=0.3
η=0.5
η=0.7
A_TOT=40
A_TOT=80
A_TOT=160
A_TOT=240
<ρ^avg/ρ_o>
<ρ^max/ρ_o>
Time (fm/c)

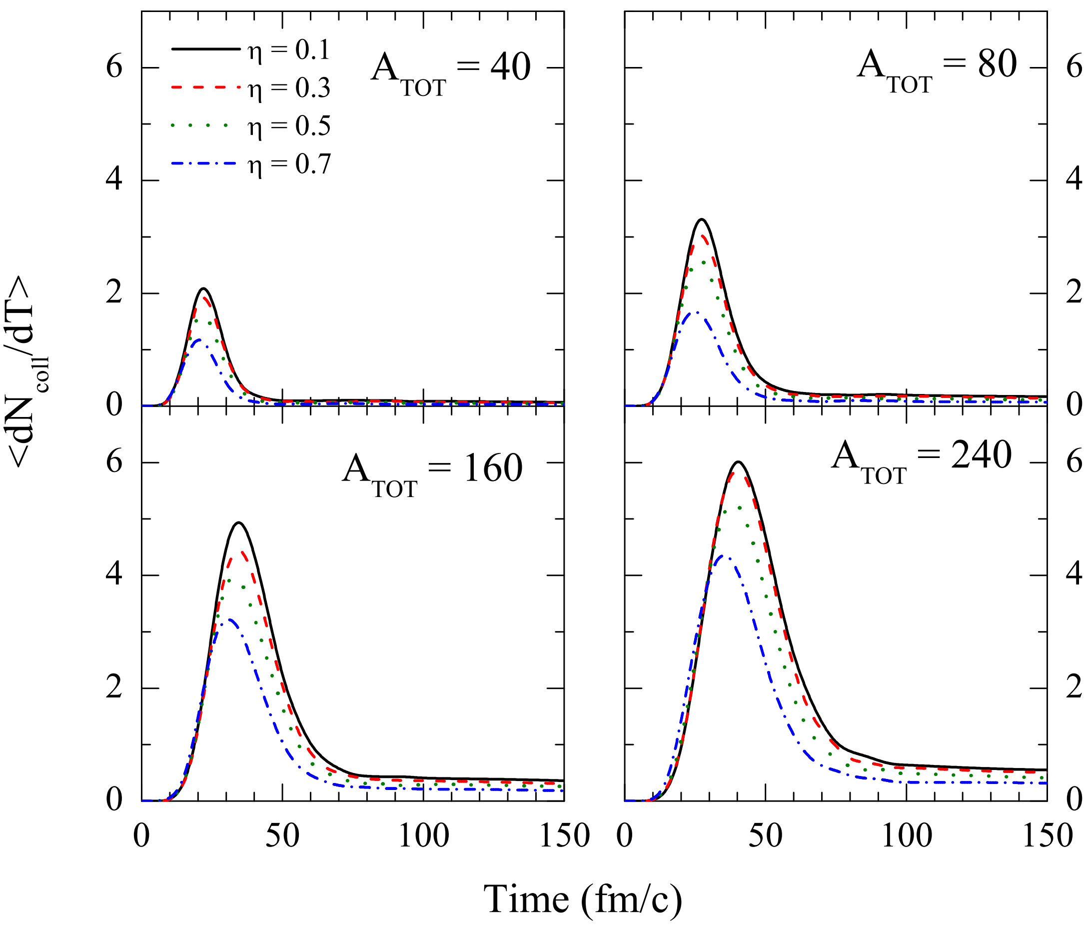

η = 0.1
η = 0.3
η = 0.5
η = 0.7
A_TOT = 40
A_TOT = 80
A_TOT = 160
A_TOT = 240
<dN_coll/dT>
Time (fm/c)
0
50
100
150
0
2
4
6

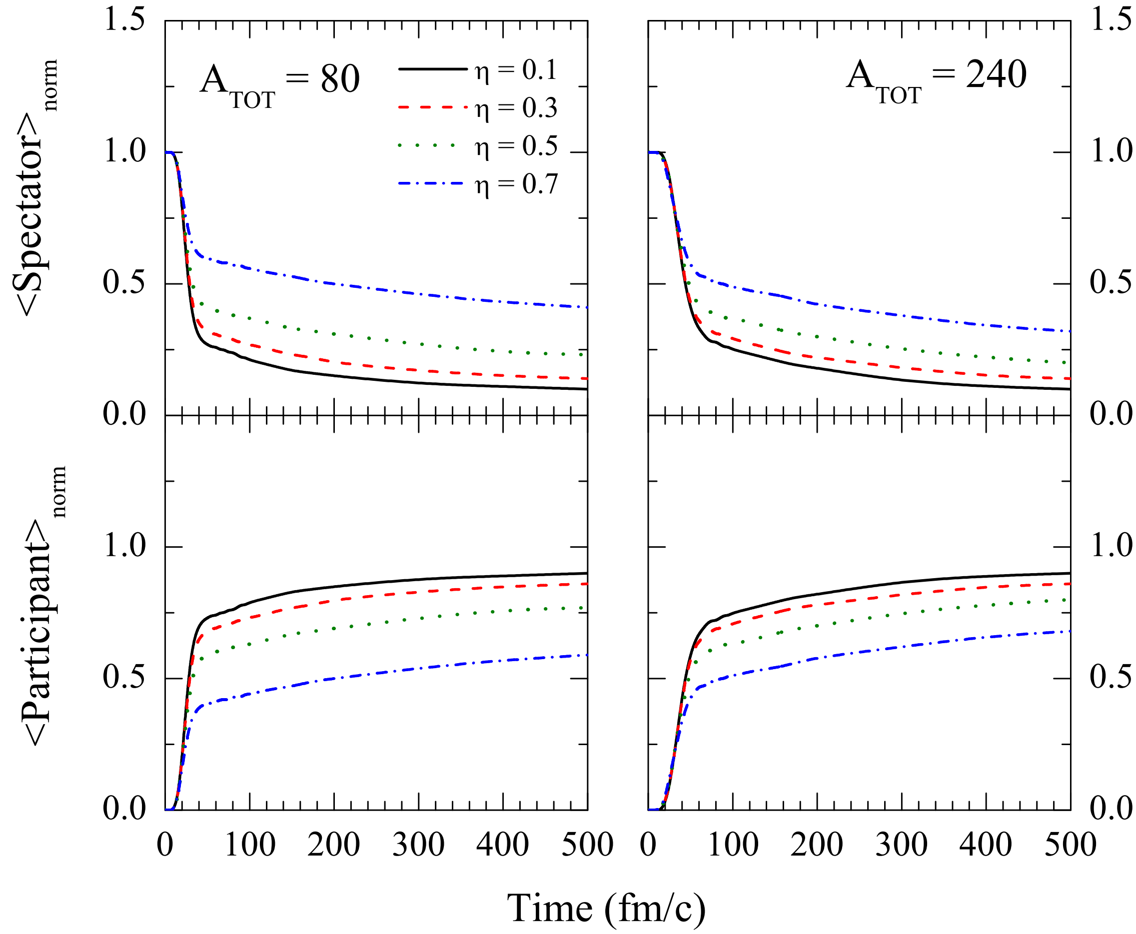

A_{TOT} = 80
A_{TOT} = 240
η = 0.1
η = 0.3
η = 0.5
η = 0.7
<Spectator>$_{norm}$
<Participant>$_{norm}$
Time (fm/c)
0
100
200
300
400
500
0.0
0.5
1.0
1.5

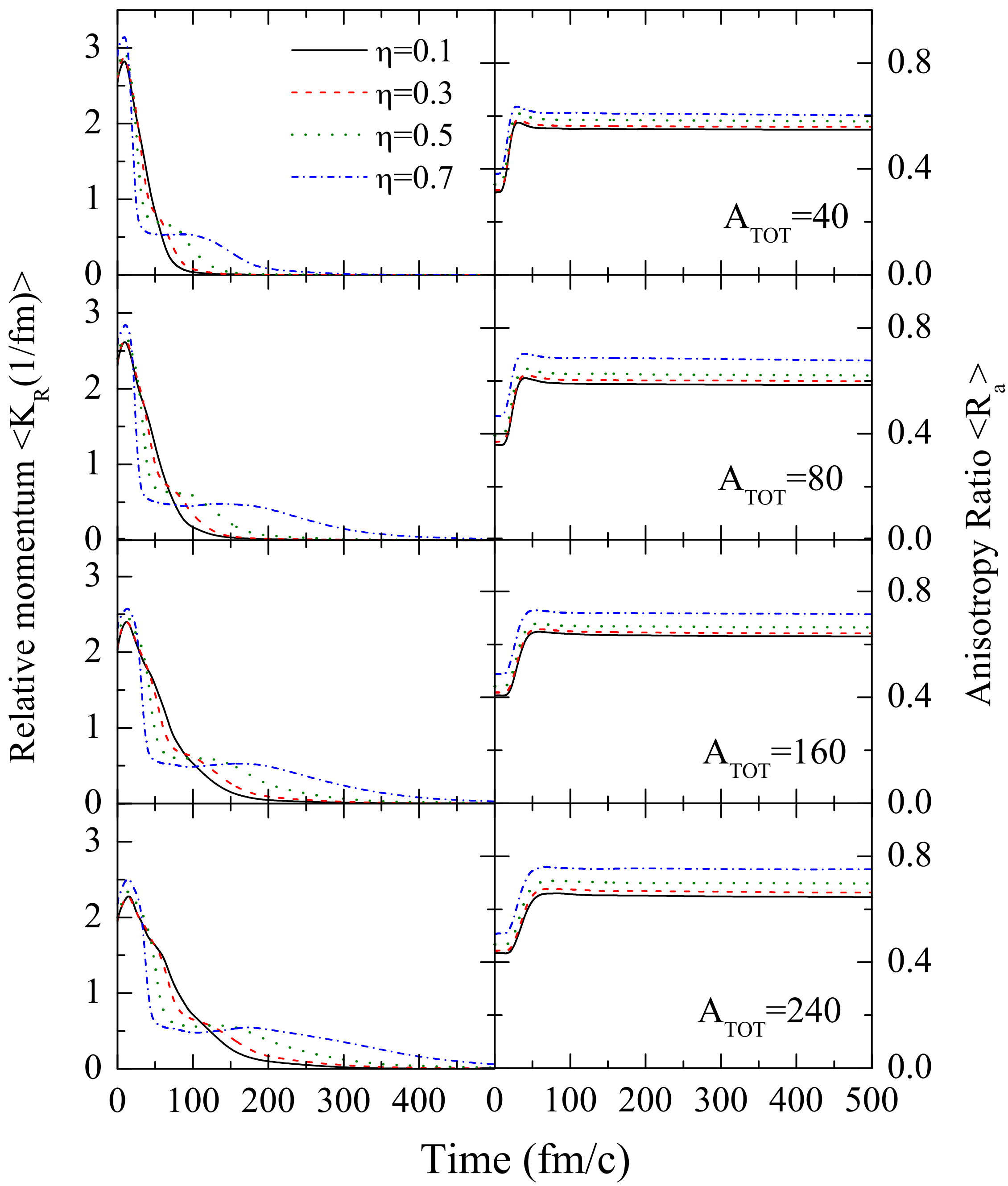

η=0.1
η=0.3
η=0.5
η=0.7
A_TOT=40
A_TOT=80
A_TOT=160
A_TOT=240
Relative momentum <K_R(1/fm)>
Anisotropy Ratio <R_a>
Time (fm/c)

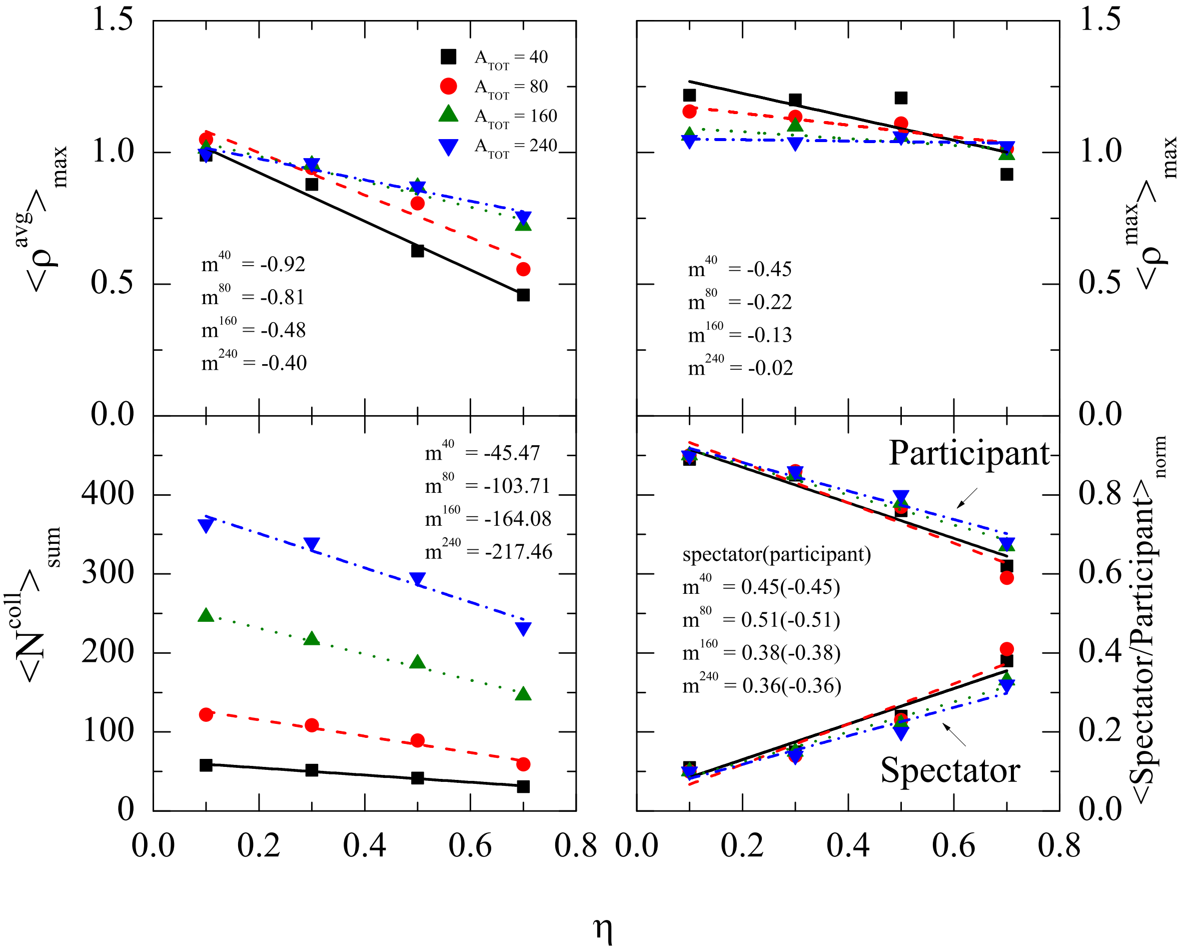

A_{TOT} = 40
A_{TOT} = 80
A_{TOT} = 160
A_{TOT} = 240
m^{40} = -0.92
m^{80} = -0.81
m^{160} = -0.48
m^{240} = -0.40
m^{40} = -0.45
m^{80} = -0.22
m^{160} = -0.13
m^{240} = -0.02
m^{40} = -45.47
m^{80} = -103.71
m^{160} = -164.08
m^{240} = -217.46
Participant
spectator(participant)
m^{40} = 0.45(-0.45)
m^{80} = 0.51(-0.51)
m^{160} = 0.38(-0.38)
m^{240} = 0.36(-0.36)
Spectator
$<\rho^{avg}>_{max}$
$<\rho^{max}>_{max}$
$<N^{coll}>_{sum}$
$<Spectator/Participant>_{norm}$
η

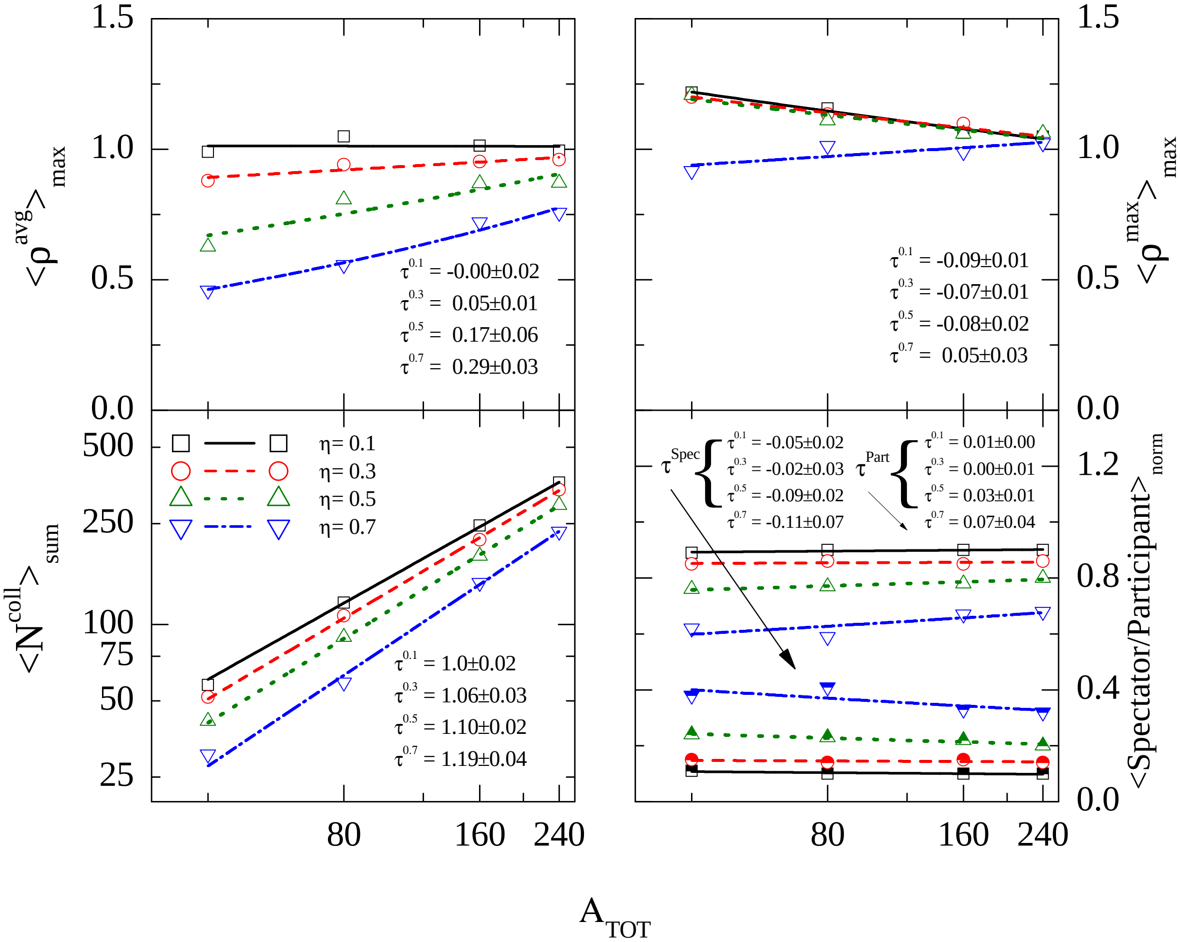

1.5
1.0
0.5
0.0
$<\rho^{avg}>_{max}$
$\tau^{0.1}$ = -0.00±0.02
$\tau^{0.3}$ = 0.05±0.01
$\tau^{0.5}$ = 0.17±0.06
$\tau^{0.7}$ = 0.29±0.03
$<\rho^{max}>_{max}$
$\tau^{0.1}$ = -0.09±0.01
$\tau^{0.3}$ = -0.07±0.01
$\tau^{0.5}$ = -0.08±0.02
$\tau^{0.7}$ = 0.05±0.03
500
250
100
75
50
25
$<N^{coll}>_{sum}$
η= 0.1
η= 0.3
η= 0.5
η= 0.7
$\tau^{0.1}$ = 1.0±0.02
$\tau^{0.3}$ = 1.06±0.03
$\tau^{0.5}$ = 1.10±0.02
$\tau^{0.7}$ = 1.19±0.04
τ^{Spec}
$\tau^{0.1}$ = -0.05±0.02
$\tau^{0.3}$ = -0.02±0.03
$\tau^{0.5}$ = -0.09±0.02
$\tau^{0.7}$ = -0.11±0.07
τ^{Part}
$\tau^{0.1}$ = 0.01±0.00
$\tau^{0.3}$ = 0.00±0.01
$\tau^{0.5}$ = 0.03±0.01
$\tau^{0.7}$ = 0.07±0.04
1.2
0.8
0.4
0.0
$<Spectator/Participant>_{norm}$
80
160
240
A_{TOT}